Journal of Geodesy (2002) 76: 63–76
DOI 10.1007/s00190-001-0231-8

Journal of Geodesy

GPS network monitors the Western Alps' deformation over a five-year period: 1993–1998

C. Vigny[1], J. Chéry[2], T. Duquesnoy[3], F. Jouanne[4], J. Ammann[5], M. Anzidei[6], J.-P. Avouac[7], F. Barlier[8], R. Bayer[2], P. Briole[5], E. Calais[9], F. Cotton[10], F. Duquenne[11], K. L. Feigl[12], G. Ferhat[13], M. Flouzat[7], J.-F. Gamond[14], A. Geiger[15], A. Harmel[16], M. Kasser[17], M. Laplanche[8], M. Le Pape[16], J. Martinod[14], G. Ménard[4], B. Meyer[18], J.-C. Ruegg[18], J.-M. Scheubel[18], O. Scotti[10], G. Vidal[19]

[1] Laboratoire de Géologie, Ecole Normale Supérieure – CNRS, 24 rue Lhomond–CNRS, 75231 Paris Cedex 05, France
e-mail: vigny@geologie.ens.fr; Tel.: +33-1-44322214; Fax: +33-1-44322200

[2] LGTS Univ. de Montpellier - CNRS, bat 22, Pl. E. Bataillon, 34095 Montpellier, France

[3] Institut Géographique National, Direction technique, Service de la Recherche, 2 avenue Pasteur, F94165 Saint-Mandé, France

[4] Laboratoire de Géodynamique des chaines Alpines, Univ. de Savoie – CNRS Batiment Belledonne, 73376 Le Bourget du Lac Cedex, France

[5] Institut de Physique du Globe de Paris, Departement de Sismologie – CNRS, 4 Place Jussieu, 75252 Paris Cedex, France

[6] Instituto Nazionale di Geofisica, via di vigna Murata, 605, 00143 Rome, Italy

[7] Laboratoire de Geophysique, CEA, BP 12, 91680 Bruyeres-le-Chatel, France

[8] Observatoire de la Cote d'Azur, CERGA-GRGS, Avenue Nicolas Copernic, 06130 Grasse, France

[9] Geosciences Azur – CNRS, 250 Rue Albert Einstein, 06560 Valbonne, France

[10] IPSN–DPRE–SERGD–BBERSSIN, BP 06, 92265 Fontenay-aux-Roses Cedex, France

[11] Ecole Superieure des Géometres Topographes Campus universitaire du Maine 1, Boulevard Pythagore, 72000 Le Mans, France

[12] CNRS, 14, Avenue Edouard Belin, 31400 Toulouse, France

[13] ENSAIS, 24 bvd de la Victoire, 67084 Strasbourg, France

[14] LGIT–BP 53, Universite Joseph Fourrier, 38041 Grenoble Cedex 9, France

[15] Geodesy and Geodynamics Laboratory, Institute of Geodesy and Photogrammetry, Swiss Federal Institute of Technology, HPV G54 ETH Hoenggerberg, 8093 Zurich, Switzerland

[16] Institut Géographique National, SGN, 2 Avenue Pasteur, 94165 Saint-Mandé, France

[17] Institut Géographique National, Cité Descartes, 6-8 Avenue Blaise Pascal, 77455 Marne-la-Vallee Cedex 2, France

[18] EDF, Direction equipement, CLI, 35–37 rue L. Guerin, BP 1212, 69611 Villeurbanne Cedex, France

[19] Laboratoire de Sciences de la Terre Ecole Normale Supérieure de Lyon 46, Allée d'Italie, 69364 Lyon Cedex 07, France

Received: 27 November 2000 / Accepted: 17 September 2001

Abstract. The Western Alps are among the best studied collisional belts with both detailed structural mapping and also crustal geophysical investigations such as the ECORS and EGT seismic profile. By contrast, the present-day kinematics of the belt is still largely unknown due to small relative motions and the insufficient accuracy of the triangulation data. As a consequence, several tectonic problems still remain to be solved, such as the amount of N–S convergence in the Occidental Alps, the repartition of the deformation between the Alpine tectonic units, and the relation between deformation and rotation across the Alpine arc. In order to address these problems, the GPS ALPES group, made up of French, Swiss and Italian research organizations, has achieved the first large-scale GPS surveys of the Western Alps. More than 60 sites were surveyed in 1993 and 1998 with a minimum observation of 3 days at each site. GPS data processing has been done by three independent teams using different software. The different solutions have horizontal repeatabilities (N–E) of 4–7 mm in 1993 and 2–3 mm in 1998 and compare at the 3–5-mm level in position and 2-mm/yr level in velocity. A comparison of 1993 and 1998 coordinates shows that residual velocities of the GPS marks are generally smaller than 2 mm/yr, precluding a detailed tectonic interpretation of the differential motions. However, these data seem to suggest that the

Correspondance to: C. Vigny

N–S compression of the Western Alps is quite mild (less than 2 mm/yr) compared to the global convergence between the African and Eurasian plate (6 mm/yr). This implies that the shortening must be accomodated elsewhere by the deformation of the Maghrebids and/or by rotations of Mediterranean microplates. Also, E–W velocity components analysis supports the idea that E–W extension exists, as already suggested by recent structural and seismotectonic data interpretation.

Key words: GPS – ALPES – Tectonics

1 Introduction

The global plate motion model NNR-Nuvel-1A (DeMets et al. 1994) predicts a N–S mean convergence rate of 6 mm/yr between the African and Eurasian plates around the Western Mediterranean region. Most of this deformation is probably accomodated in the active mountain belts showing important seismicity and topography: the Pyrenees, Alps, Apennines and Maghrebids. In these structures, the deformation may be complex as focal mechanisms show compressive directions far from the overall direction of convergence and even extension (internal Western Alps, Southern Apennines or Eastern Pyrenees). A regional GPS network embedded in an interplate fiducial network is the best way to measure the partition of crustal deformation within mountain belts and place them in the tectonic framework of global plate motions. As a first step towards mapping the distribution of the African–Eurasian motions within the Mediterranean region, we have installed and measured twice (1993 and 1998) a high-precision GPS network in the Western Alps, one of the largest, highest, and most deformed ranges in the Alpine collision zone.

2 Measurement campaigns and additional data

The first GPS campaign was conducted during September 1993. Fifty sites were measured with 23-dual frequency receivers (22 Ashtechs and 1 Rogue). Forty sites were observed in three phases of four 12-hour sessions (Fig. 1) and six sites were measured for six 12-hour sessions. Continuous measurements were made at the three remaining sites during the 12 days of the campaign. The main interest of those three sites and the six previous ones is to link sites which were not measured simultaneously. This is the classic scheme when there are more sites to measure than receivers available. Finally, 700 baselines out of the possible 1250 have been actually measured at least four times. Independent measurements were conducted by Swiss (with Leica SR299) and Italian (with Wild-102) teams in their respective countries at the same epoch. Those measurements are included in a single and common solution. Thanks to reasonnable weather conditions, almost all planned observations were conducted. Because of the absence of Anti Spoofing (AS) at the time, most of the data include precise P-code observations.

Fifteen of our sites belong to the French Reference network (RRF) and 25 other sites were tied immediately after this campaign by GPS measurements to the closest sites belonging to the French geodetic network (NTF). This classical triangulation network has been maintained by the French mapping agency (IGN) since the 1950s. Comparisons with these earlier measurements were made and yield small deformation of a couple of mm/yr over this period Ferhat et al. 1998; Calais et al. 2000; Sue et al. 2000;

The second GPS campaign was carried out during July 1998 and conducted under the same planning as the 1993 campaign. Only Ashtechs equiped with choke-ring antennas were used and daily sessions were extented to 24 hours instead of 12. Also, the network of continuously operating stations has been greatly increased in the meantime. In 1993, data from six International GPS Service for Geodynamics (IGS) stations (Neilan 1995) (Graz, Hersmontceux, Madrid, Matera, Wettzell and Zimmerwald) were merged with the Alpine data. In 1998, 13 additional permanent IGS stations were available in the area (Bruxelles, Cagliari, Ebre, Grasse, Hafelekar, Kootwijk, Medicina, Noto, Padova, Pecny, Torino, Toulouse and Venezia) and added to the data set. We also used data from the three newly installed permanent stations for the French REGAL network (SJDV, FCLZ, GINA) (Calais et al. 2000). Since an increasing number of permanent stations around the Alpine area is available, we also introduced campaign-like data from this network. We sampled six GPS weeks since 1993, regularly spaced every year after the first campaign (0758 in 1994, 0804 in 1995, 0860 in 1996, 0911 in 1997, 1016 in 1999, 1049 in 2000). The latest data set included all permanent stations used during the 1998 campaign, plus 26 new stations in Austria, France, Germany, Italy, Spain and Switzerland (AJAC, BRST BZRG, CHAT, DAVO, EPFL, ETHZ, FHBB, GENO, JUJO, KARL, LAMP, MANS, MARS, MICH, MLVL, MODA, MTPL, NEUC, OBER, PFAN, SAUV, SBGZ, SFER, STJ9 and VILL), bringing the total to 48.

3 Campaign data processing

The bulk of the GPS data analysis described here is conducted with the GAMIT/GLOBK software from Massachussetts Institute of Technology (Herring 1999; King and Bock 1999). Two types of solutions are determined, one using the IGS combined orbits (Beutler et al. 1993) held fixed in the process, and one re-estimating satellite ephemerides. No meteorological field data is used to compute the wet component of the troposphere-induced propagation delays; we instead use the data itself to estimate one 'tropospheric parameter' every two hours. We also used elevation-dependent

models described in the IGS tables (Rothacher and Mader 1996) for the modeling of antenna phase center variations. Fixing phase ambiguities to integer values is attempted when possible and statistics of both types of solution (solved and unsolved ambiguities) are shown.

Data are first processed on an independent daily session basis. Using approximate input station positions (and satellite ephemerides when not using precise IGS combined orbits), we compute a first solution for every day. This solution enables us to 'clean' the data, i.e. detect and repair all cycle slips, and unweight bad data (contaminated with heavy multipath, for example). Each of these solutions provides an independent estimation of the baseline components. Repeatabilities (i.e. the RMS of the daily independent measurements about their mean value) are a first insight into what the precision of the measurements really is. They reach mean values of 4 mm (north component), 7 mm (east component), and 13 mm (vertical component) in 1993, and 4, 4, and 8 mm in 1998. The improvement from 1993 to 1998 is spectacular for the east and vertical component. It is mainly due to the increased number of satellites in the GPS constellation which give a better sky coverage and to the systematic use of choke-ring antennas. In 1993, 10% of the baselines give repeatabilities worse than 10 mm. This number reduces to 0.5% in 1998. 1 summarizes the numbers obtained for the different solutions. As expected, ambiguity fixing slightly improves the east component's repeatability (by 1 mm). The average number of solved ambiguities ranges from 54 to 96% in

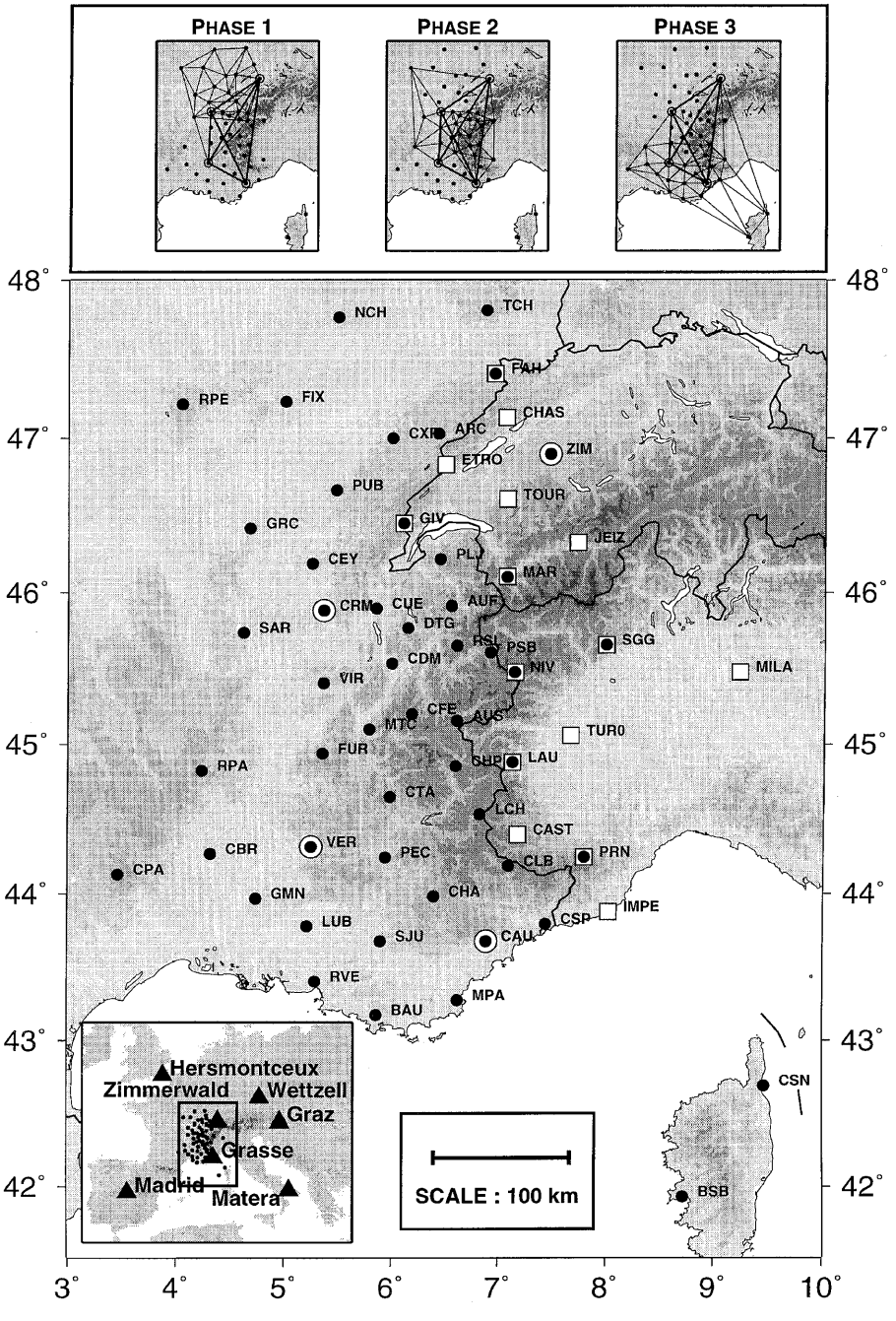

Fig. 1. GPS ALPES network. *Circled dots* show the location of permanent stations during the whole campaign. *Black dots* show French sites, *open squares* show Italian and Swiss sites. Lower inset shows the IGS stations used in the analysis. Upper insets show the three phases of the measurement campaign. Stations measured during a given phase are linked by straight lines

1993 and from 84 to 100% in 1998, again showing an improvement we attribute to the use of choke-ring antennas in 1998. With these specially designed antennas, multipath effects and antenna phase center azimuth-dependent motions are largely reduced. A more stable antenna phase center and less noisy data both concur to improve the efficiency of 'bias-fixing' schemes.

The degradation of repeatability with baseline length is mild (less than 3 ppb in 1993 and around 1 ppb in 1998), indicating that the reference frame is stable and satellite orbits are accurate (Fig. 2). This is true whether IGS fixed orbits are used or orbits are re-estimated.

Little can be done to reduce the relatively high level of the vertical component scattering (14 mm in 1993 and 8 mm in 1998). The fact that this value is rather independent of station elevation differences (less than 1 ppm for both campaigns), in spite of the large elevation differences between sea level and high Alpine ranges, indicates that tropospheric differences are well taken into account by estimation of 'ad hoc' parameters in the inversion (Fig. 3).

In order to investigate the effect of mixing different antennas, some sites in the network were measured by the different types of equipment. In 1993, three Italian and three Swiss points were measured both by French teams using Ashtechs and Italian (or Swiss) teams using Wild (or Leica) receivers and antennas. Comparisons of station coordinates show a relatively good agreement (within the repeatabilities of each component), except for a systematic vertical difference of about 5 cm between Ashtechs and Wilds on the Italian stations (Table 2). Therefore, only horizontal coordinates are constrained to be the same when heights are downweighted in the final combination.

Another cause of error may be due to antenna phase centers that could also be offset (by up to 1 cm) from their expected nominal position, in reference to an identical antenna, calibrated in anechoic chamber. Such a behavior could be due to mismounting in the factory or mishandling of the antennas on the field. In order to address this problem, we conducted a calibration campaign of a large part of the antennas which were used in the Alps campaigns. Antennas were set on a testing bench at regular intervals of 70 cm, and measurements carried out for 24 hours. Positions offsets were then estimated in comparison to a position obtained with a reference choke-ring antenna previously set in the same slot. Most of the antennas give an offset smaller than a

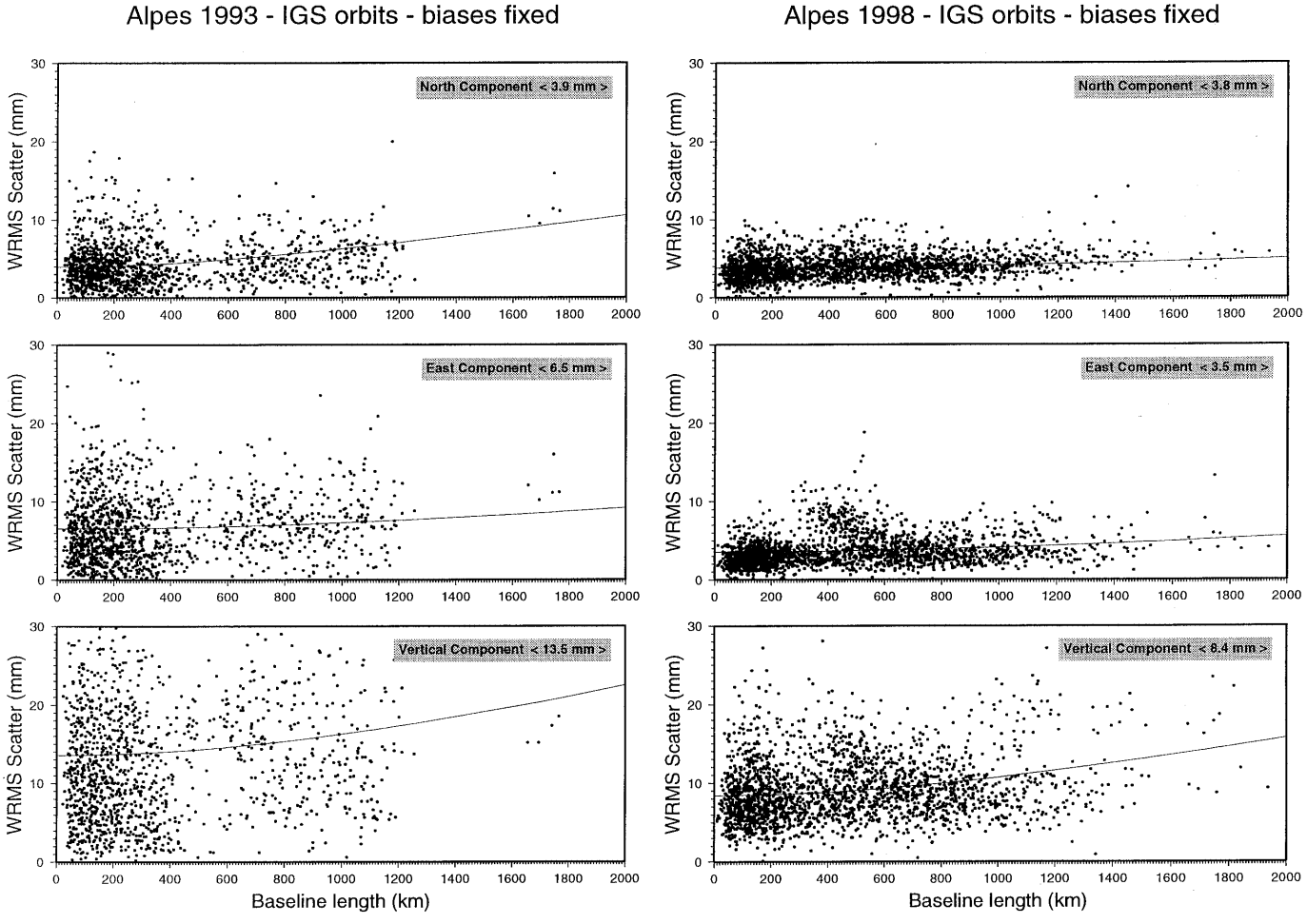

Fig. 2. Baseline component repeatabilities versus baseline length. 1993 in left column, 1998 in right column. First, second, and third row are for north, east and vertical components. In each box, the *thin line* shows a running average through the cloud of points. The values inside brackets (upper right corner) are the average number for the shortest baselines

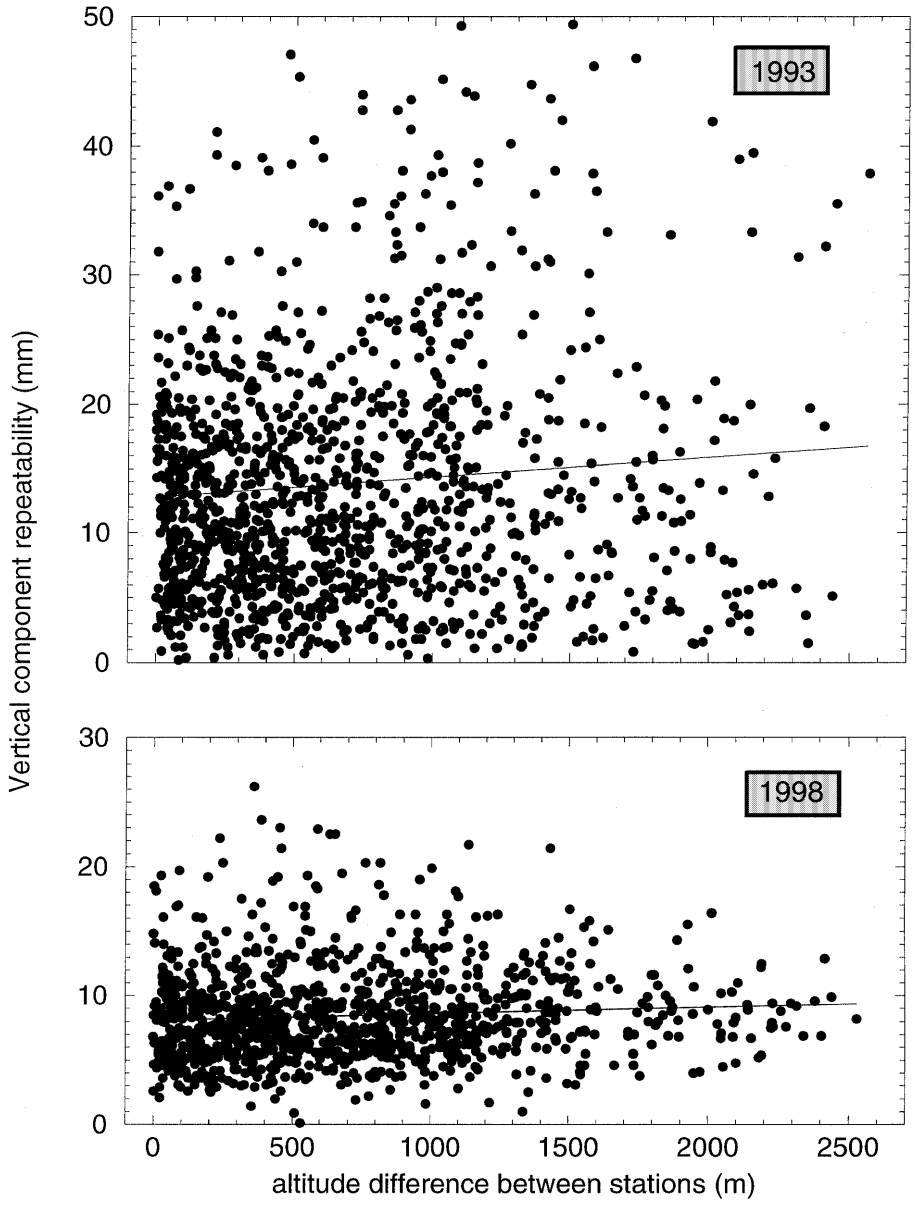

Fig. 3. Baseline vertical component repeatability as a function of station elevation difference. The *thin line* represents the linear regression through the cloud of points and indicates the tendancy as a function of height difference (no more than 1 ppm)

Table 1. Statistics for different solutions

Solution type	Mean repeatability (mm)			Solved ambiguity [daily range] ⟨average⟩ in %
	North	East	Up	
1993 IGS orbit – free ambiguity	3.6	7.4	13.4	
– fixed ambiguity	3.9	6.5	13.5	[60–96] ⟨75⟩
Re-estimated orbit – free ambiguity	3.7	7.1	13.0	
– fixed ambiguity	3.8	7.1	12.8	[54–96] ⟨75⟩
1998 IGS orbit – free ambiguity	3.9	4.9	9.2	
– fixed ambiguity	3.8	3.5	8.4	[87–100] ⟨96⟩
Re-estimated orbit – free ambiguity	3.6	4.0	8.7	
– fixed ambiguity	3.7	2.9	8.4	[84–100] ⟨95⟩

couple of mm, with the notable exception of one geodetic type 2 antenna which yields an offset of about 1 cm (+6 mm in latitude, +9 mm in longitude, giving 11 mm towards N240°). Such a large error, affecting the 1993 site position, would lead to an incorrect estimate of the site velocity of about 2 mm/yr after a 5-year period. In 1993, only four sites (CPA, CBR, RSL and PSB) were measured using this antenna and a 'sister-ship' antenna with the following serial number (not calibrated). Those four sites were also only measured with those antennas,

Table 2. Coordinate differences at same points observed with different equipment

Station name		Coordinate differences (mm)		
Sw/It	Fr	North	East	Height
GIVR	GIV0	0.5	8.1	18.8
MART	MAR1	1.8	1.2	13.3
FAHY	FAH0	6.3	7.0	18.5
NIVO	NIV0	2.8	11.6	40.2
PRAT	PRN0	4.1	12.9	68.1
SANG	SGG0	6.7	6.5	53.6

Table 3. Corrections applied due to offset antenna phase centers

Site	Raw velocity (mm/yr)		Raw displacement (mm)		Corrected displacement (mm)		Corrected velocity (mm/yr)	
	East	North	East	North	East	North	East	North
CPA0	−3.0	−0.5	−15	−3	−6	3	−1.2	0.5
CBR0	−3.9	−1.0	−20	−5	−11	1	−2.2	0.2
RSL0	−1.8	−1.6	−9	−8	0	−2	0.0	−0.4
PSB0	−2.4	−2.0	−12	−10	−3	−4	−0.5	−0.8

and eventually all of them showed a suspiciously correlated motion of about 2 to 3 mm/yr towards WSW after re-measurement (Table 3). Thus, we decided to apply this correction to those two antennas, and the corresponding four sites, which largely reduces their motion.

Comparisons with independent processing done with the BERNESE software (Rothacher and Mervart 1996) have also been carried out. Basically, the differences for the 1998 data set are quite small. The residuals of a seven-parameter Helmert transformation between GAMIT and BERNESE solutions reach about 2 mm on average for the horizontal components, and 5–10 mm for the heights. As expected, differences are somewhat larger for the 1993 data set and reach 4–7 mm for the horizontal components and 10–20 mm for the heights (Table 4). A few sites do show high residuals in 1993 (larger than 10 mm) on the eastern component: BSB, CDM, CEY, FIX, GMN, MTC and SJU. These can be attributed to ambiguity resolution differences and indicate sites on which motions should be analyzed with care. Nevertheless, for most of the sites the processing differences remain largely within the repeatabilities. Therefore we consider we have established the robustness of our preferred solution at the level of 4, 7 and 13 mm for the north, east and vertical station position components in 1993, and 4, 4 and 8 mm in 1998.

4 Velocities

The campaign data are combined along with 1 week of European continuous data every year to infer site velocities. At least two strategies are possible to map station positions and velocities in a chosen reference frame, here the International Terrestrial Reference Frame 1997 (ITRF97) (Boucher et al. 1999). The first strategy consists of constraining fiducial station parameters to their known ITRF97 values. The second one consists of adjusting in an LS sense a subset of station parameters (positions and velocities) to a reference model (ITRF97 again). In addition, when using the IGS fixed-orbit solutions, we estimated reference frame offsets and rotations and Earth rotation parameter adjustments in order to take into account the different orbit references between the campaigns (ITRF91 in 1993 and ITRF96 in 1998). The two methods and the different kinds of solutions give slightly different values (at the 1–2-mm/yr level) for the overall mapping in the global reference frame, but keep the internal deformation pattern untouched. Therefore, only one solution is presented here. It corresponds to the GAMIT/GLOBK solution, computed with fixed IGS orbits, and position and velocity LS adjustment on a subset of stations.

A few sites observed in 1993 were moved to new locations or different geodetic monuments afterwards. At those locations, ties were applied in order to extract velocities from the 1993–1998 positions comparison (Table 5). Ties are in general accurate, at least in distance, but they still introduce a higher level of uncertainty on the corresponding site motions.

We used 16 sites with well defined positions and velocities in ITRF97, and exhibiting long enough GPS time series (over 3 years): BRUS, CAGL, EBRE, GOPE, GRAS, GRAZ, HERS, HFLK, KOSG, MATE, MEDI, NOTO, UPAD, VENE, WTZR and ZIMM. We excluded the Madrid site (MADR = DS60) from the reference definition since we were unable to achieve a good fit for this station. The final overall fit on the 16 stations is 2.1 mm in position and 0.7 mm/yr in velocity, demonstrating an accurate mapping in ITRF97.

4.1 European velocities

Velocities obtained in ITRF97 are shown in Table 6. These velocities mainly show the European plate

Table 4. Helmert residuals between individual solutions (mm)

Site	1993						1998					
	Bern1/Gamit			Bern2/Gamit			Bern1/Gamit			Bern2/Gamit		
	North	East	Up	North	East	Up	North	East	Up	North	East	Up
ARC0	−2	2	2	−1	1	−13	−2	−2	3	−1	−2	1
AUF0	4	1	−3	1	6	−3	−2	1	4	−2	1	6
AUS0	1	2	12	2	2	28	1	−2	−6	2	−3	6
BAU0	3	−9	−18	3	−9	8	2	0	7	1	0	−2
BSB0	4	10	−38	−6	18	−5	1	1	14	2	2	9
CBR0	−2	7	12	−1	0	−2	3	0	−6	1	3	9
CDM0	−1	−17	4	1	−12	−7	−1	1	−4	0	0	1
CEY0	−7	−13	4	−5	−13	−4	−1	−1	2	0	−3	2
CFE0	0	7	11	−3	10	24	1	−2	−1	1	−2	2
CHA0	0	0	2	1	−3	57	2	0	−1	3	0	0
CHP0	5	8	−3	4	9	9	1	2	−6	1	1	5
CLB0	4	5	6	2	10	6	1	0	8	2	−1	7
CPA0	−4	8	10	−3	3	−16	2	−1	−3	−1	3	4
CRGA	7	1	−17	1	−8	−71	1	−2	4	1	2	−44
CRM0	6	2	14	3	4	−14	2	−1	42	2	1	14
CSN0	4	−8	11	6	0	5	−4	−2	9	−2	0	14
CSP0	2	4	−1	−1	6	0	3	0	0	4	1	−3
CTA0	−1	−9	−5	−3	−12	16	1	0	3	1	0	7
CUE0	0	0	−18	−3	4	16	1	1	3	0	1	5
CXP0	3	−1	11	3	4	8	−3	−2	4	0	−3	5
DTG0	4	1	2	3	5	4	−1	0	5	−1	0	6
FAH0	5	−1	−16	6	2	−15	−3	0	2	0	−1	1
FIX0	1	10	−12	1	7	−5	−3	−1	4	−2	−4	2
FUR0	2	4	−22	1	8	2	1	0	−1	1	1	4
GIV0	−3	−6	−29	−4	−7	10	−1	−2	7	−1	−3	5
GMN0	−3	13	11	−2	11	−34	2	1	1	3	0	7
GRAZ	−2	3	1	−3	−8	−52	−1	2	8	−2	4	−31
GRC0	−5	−2	26	−2	−1	2	−2	−1	0	−1	−4	0
LAU0	2	−1	19	3	−3	21	1	−2	4	0	0	8
LCH0	3	1	8	3	1	14	1	0	3	0	−2	11
LUB0	2	8	4	−4	8	8	2	−1	4	2	0	7
MAR1	−3	−1	−29	1	−4	−2	−1	−1	5	0	−1	4
MPA0	2	−3	−11	−1	−1	21	1	1	11	1	1	2
MTC0	−4	−20	2	−3	−18	25	0	0	−5	−1	−1	5
NCH0	7	−3	2	5	1	−7	−2	−1	6	1	−3	−3
NIV0	2	5	8	7	−1	24	−1	−2	1	−4	1	3
PEC0	4	6	5	0	6	5	0	2	−3	1	2	−2
PLJ0	7	−2	−6	4	3	7	1	2	8	0	2	3
PRN0	0	2	2	−2	6	3	−3	−3	−84	4	1	−26
PSB0	−1	5	26	2	7	12	1	0	7	1	−1	1
PUB0	−10	−7	0	−5	−7	−2	−2	−1	3	0	−2	2
RPA0	3	1	−9	1	1	4	1	−1	−3	1	0	0
RPE0	−2	0	6	−3	1	−9	−2	0	4	0	−4	−5
RSL0	−1	4	23	3	8	4	0	0	0	−1	1	6
RVE0	−2	−7	0	−2	−5	6	0	0	6	0	0	1
SAR0	−9	−5	−5	−1	1	65	−1	0	4	−1	−2	3
SGG0	−1	1	−8	3	1	15	−1	−4	−6	−2	−2	7
SJU0	−2	−10	4	1	−8	2	2	1	0	1	1	1
TCH0	−3	1	−3	−2	4	0	−3	1	3	1	0	−3
VER0	0	4	−11	4	6	8	2	−1	5	1	0	4
VIR0	−2	−3	−10	−3	−13	28	−1	0	9	−2	1	2
ZIMM	−2	2	4	2	−8	−47	−2	−2	−6	−8	7	−41
Mean sigma	4	6	13	4	7	26	2	2	5	2	2	12

Table 5. Applied ties

New to old site	dX (m)	dY (m)	dZ (m)	Origin
WTZR → WTZ1	−2.105	−0.981	1.994	Wettzell.log (IGS)
MAS1 → MASP	−3.120	0.845	9.563	MAS19705.log (IGS)
GRAS → CRGA	6.639	11.081	−9.235	SGN/IGN internal report, February 95
TORI → TUR0	73.524	51.202	−57.015	tori.log (IGS)

Table 6. ALPES stations' position and velocity in ITRF97 (reference date 1997.0)

Site	Position (m)			Velocity (mm/yr)			Position			Velocity (mm/yr)	
	X	*Y*	*Z*	*vX*	*vY*	*vZ*	Longitude (°)	Latitude (°)	Height (m)	E velocity	N velocity
ARC0	4327637.0458	483386.5993	4645858.7691	−11.8	15.5	11.0	6.373	47.046	856	16.7	14.8
AUF0	4411566.7977	501671.3480	4565934.5223	−11.0	18.9	11.8	6.488	45.993	1660	20.0	14.6
AUS0	4469991.6790	528388.5037	4505949.6841	−9.0	19.0	12.1	6.742	45.223	1549	19.9	13.2
BAU0	4635383.8732	478218.9119	4341171.3315	−11.0	17.1	12.4	5.890	43.163	596	18.2	15.3
BSB0	4690570.6901	720488.4303	4247946.8757	−10.9	16.2	10.9	8.733	42.024	516	17.7	13.7
CBR0	4572389.8323	342724.1824	4419514.5095	−9.0	15.7	12.5	4.287	44.138	573	16.4	14.5
CDM0	4452029.8527	473027.8464	4529028.3226	−13.7	17.1	10.0	6.065	45.523	1098	18.5	15.5
CEY0	4403081.9820	411718.9557	4581479.2913	−10.2	18.6	11.4	5.342	46.205	581	19.4	14.0
CFE0	4474929.9595	486692.5224	4506520.1409	−7.9	20.1	15.1	6.207	45.225	2099	20.9	14.7
CHA0	4569064.9886	506633.1568	4407835.2807	−9.1	17.1	11.4	6.327	43.988	966	18.0	13.2
CHP0	4509438.5167	519370.4051	4467268.8662	−10.2	19.0	11.3	6.570	44.734	1184	20.1	13.6
CHS0	4315057.3222	534231.5193	4653025.9953	−9.5	17.6	13.4	7.058	47.133	1647	18.6	14.4
CLB0	4545841.7339	570530.5146	4426056.3087	−9.6	17.4	11.1	7.154	44.204	2468	18.4	13.1
CPA0	4578753.5592	292679.2946	4417024.5491	−6.8	17.9	15.2	3.657	44.104	908	18.3	14.8
CRM0	4437372.3520	424905.2352	4546867.4490	−8.4	18.9	13.9	5.470	45.760	275	19.6	14.4
CSP0	4573550.3185	594033.0155	4392007.2373	−11.5	18.3	9.3	7.400	43.793	730	19.6	12.9
CTA0	4519394.4049	467927.7655	4463696.0787	−9.9	17.6	12.7	5.911	44.684	1730	18.5	14.6
CTE0	4344230.8446	494595.6430	4629768.1541	−5.6	18.2	16.3	6.495	46.830	1216	18.7	13.7
CUE0	4426397.8026	446308.4929	4557130.6108	−9.7	18.4	11.2	5.758	45.881	1483	19.3	13.4
CXP0	4338074.7298	447246.3655	4639756.2930	−12.3	16.3	10.0	5.886	46.965	838	17.4	14.6
DTG0	4430571.4438	474166.4677	4550523.6163	−10.9	18.4	12.1	6.109	45.794	1642	19.5	14.8
FAH0	4292927.6166	523198.2208	4673177.6011	−13.4	17.2	9.1	6.949	47.410	633	18.7	14.4
FIX0	4322023.2145	374719.3604	4660491.1682	−11.7	17.4	11.9	4.955	47.243	487	18.3	15.6
FUR0	4507624.1631	419959.2095	4479977.7605	−10.1	17.6	11.5	5.323	44.892	1555	18.4	14.1
GIV0	4377795.3846	468008.7431	4601077.4110	−13.9	17.7	9.7	6.102	46.454	1258	19.0	15.4
GMN0	4581609.3648	382021.1974	4406332.9402	−8.1	18.1	13.4	4.766	43.976	240	18.7	14.3
GRAS	4581691.0215	556114.6866	4389360.6852	−13.4	17.9	8.8	6.921	43.755	1319	19.3	14.0
GRC0	4387736.5950	361865.0003	4600212.7452	−9.3	16.2	13.2	4.715	46.449	557	16.9	14.8
JEI0	4373207.3152	593076.5703	4591517.5121	−7.8	18.4	12.5	7.723	46.326	1577	19.3	12.5
LAU0	4493388.3303	561423.4859	4479893.1758	−11.5	19.3	9.9	7.122	44.884	2332	20.6	13.4
LCH0	4523164.0436	538107.1352	4451982.8242	−11.8	19.0	8.7	6.784	44.537	1695	20.2	12.8
LUB0	4592493.8388	413886.0995	4392859.7501	−8.4	19.2	12.3	5.150	43.804	699	19.8	13.4
MAR1	4396673.0620	545197.0803	4573757.7713	−12.1	17.8	10.9	7.069	46.105	593	19.1	14.6
MAZ0	4637020.7119	759485.3908	4298873.7422	−12.9	17.6	11.4	9.302	42.647	235	19.5	15.0
MPA0	4624695.2142	535180.8425	4345554.8924	−10.9	17.2	13.7	6.601	43.219	368	18.4	16.1
MTC0	4487447.7276	453241.2678	4495752.6389	−11.1	17.0	13.2	5.767	45.100	781	18.0	15.9
NCH0	4274168.7746	401579.2683	4701942.1074	−13.3	17.4	7.2	5.367	47.795	501	18.5	13.4
NIV0	4446890.7382	557268.0706	4526744.0888	−10.1	19.6	11.1	7.143	45.479	2681	20.7	13.2
PEC0	4551677.7415	482549.6206	4428781.2989	−9.6	16.8	11.6	6.052	44.248	1274	17.7	13.7
PLJ0	4395240.5758	498095.5748	4581455.9861	−12.5	19.4	8.9	6.466	46.198	1315	20.7	13.6
PRN0	4535050.4732	620315.7320	4429287.6638	−12.9	20.7	9.7	7.789	44.251	1694	22.3	13.9
PSB0	4435627.7631	534086.1509	4540125.2464	−10.6	17.9	11.9	6.866	45.653	2430	19.0	14.3
PUB0	4365490.9776	431384.4300	4615271.0844	−12.4	17.7	11.0	5.643	46.646	567	18.9	15.2
RPA0	4523446.4576	348957.5202	4469577.2609	−11.1	18.6	11.2	4.411	44.764	1131	19.4	14.7
RPE0	4321891.8147	302780.6114	4665953.2540	−13.8	18.0	8.6	4.007	47.314	597	18.9	15.1
RSL0	4434260.4763	515276.8141	4542579.9673	−13.9	17.5	8.9	6.628	45.692	1693	19.0	14.6
RVE0	4623892.8816	428125.7867	4358109.1597	−10.2	16.3	11.8	5.290	43.375	325	17.2	14.5

SAR0	4434455.8267	352005.2303	4556019.9913	−11.0	18.8	10.6	4.539	45.877	382	19.6	14.2
SGG0	4422939.8016	620963.8989	4539576.7561	−13.5	17.0	8.6	7.992	45.658	1095	18.7	13.8
SJU0	4595026.0315	475226.8820	4383934.0845	−9.0	17.0	12.3	5.905	43.693	616	17.8	13.9
TCH0	4252975.4814	509186.4701	4711404.9570	−12.9	17.6	10.7	6.827	47.916	1046	19.0	15.1
TRE0	4356617.5767	540142.1739	4612546.2280	−11.0	18.4	12.5	7.068	46.608	798	19.6	14.9
VER0	4552716.6881	425761.0330	4432653.7223	−11.3	17.2	9.8	5.343	44.302	681	18.2	13.8
VIR0	4476985.1677	407507.7861	4510184.9098	−13.0	18.4	11.9	5.201	45.286	601	19.5	16.4

rotation, which at this position is mainly an east-northeast motion of about 20 mm/yr. Deviations from this overall motion are representative of the plate's internal deformation. Since the purpose of this paper is not to estimate a geodetic motion of the Eurasian plate, we simply subtracted the motions generated by the Eurasian plate rotation described by the NNR-Nuvel-1A model. In doing so, we also neglect a possible misalignment between ITRF97 and NNR-Nuvel-1A.

Figure 4 depicts the large-scale deformation pattern inferred from the European permanent station (including IGS, REGAL, RGP and other networks) motions. The agreement with ITRF97 velocities (when existing) is quite good and is detailed in Table 7. For most stations (19 out of 27), the difference between our estimate and ITRF97 is less than 1 mm/yr. Only a few sites show significant differences (>1.5 mm/yr): GENO, MTPL, VENE, OBER and SJDV. All those stations are relatively recent and the time series from which the site velocity is determined can be quite short, especially given the fact that ITRF97 includes GPS data until mid 1998 only. With respect to this matter, SJDV velocity is determined from only 6 months of data in ITRF97. Using only well determined site velocities (Fig. 4, white arrows), the pattern clearly depicts a stable Central and Northern Europe with extremely small residual velocities in Belgium (BRUS), The Netherlands (KOSG), Great Britain (HERS), Czech Republic (GOPE) and Germany (WTZR). The motion of Italy is well determined and matches well a counterclockwise rotation induced by the northward motion of the African plate (Thomas et al. 1999). With this respect, our determination of the velocity at VENE is in better agreement with nearby sites (MEDI and UPAD) and local tectonics than the ITRF97 determination. Finally, the three points immediately north of the mountain belt ranges, ZIMM in Switzerland, HFLK and GRAZ in Austria, show little motion relative to the European plate. Nevertheless, the baseline from WTZR to GRAZ clearly shows a 2-mm/yr east–west extension. The more recent sites show high uncertainties (Fig. 4, white arrows). Our determination of OBER velocity is clearly in error and inconsistent with both ITRF97 and motions in the area (ZIMM, HFLK and WTZR). Finally, the ITRF97 determination of SJDV is clearly wrong, due to the very short time span used (6 months). Nevertheless, most points immediately west of the Alpine ranges (SJDV, FCLZ, MICH, MARS and MTPL) consistently show a western motion relative to stable Europe of about 1–2 mm/yr. This result is consistent with previous findings (Calais et al. 2000), but should be interpreted with great care given its small magnitude.

4.2 Alpine velocities

The smaller-scale deformation pattern within the Western Alps ranges is given by velocities of the ALPES 1993–1998 sites (Fig. 5). At the new REGAL or RGP permanent sites, the comparison between our simulated campaign velocities and continuous time series velocities

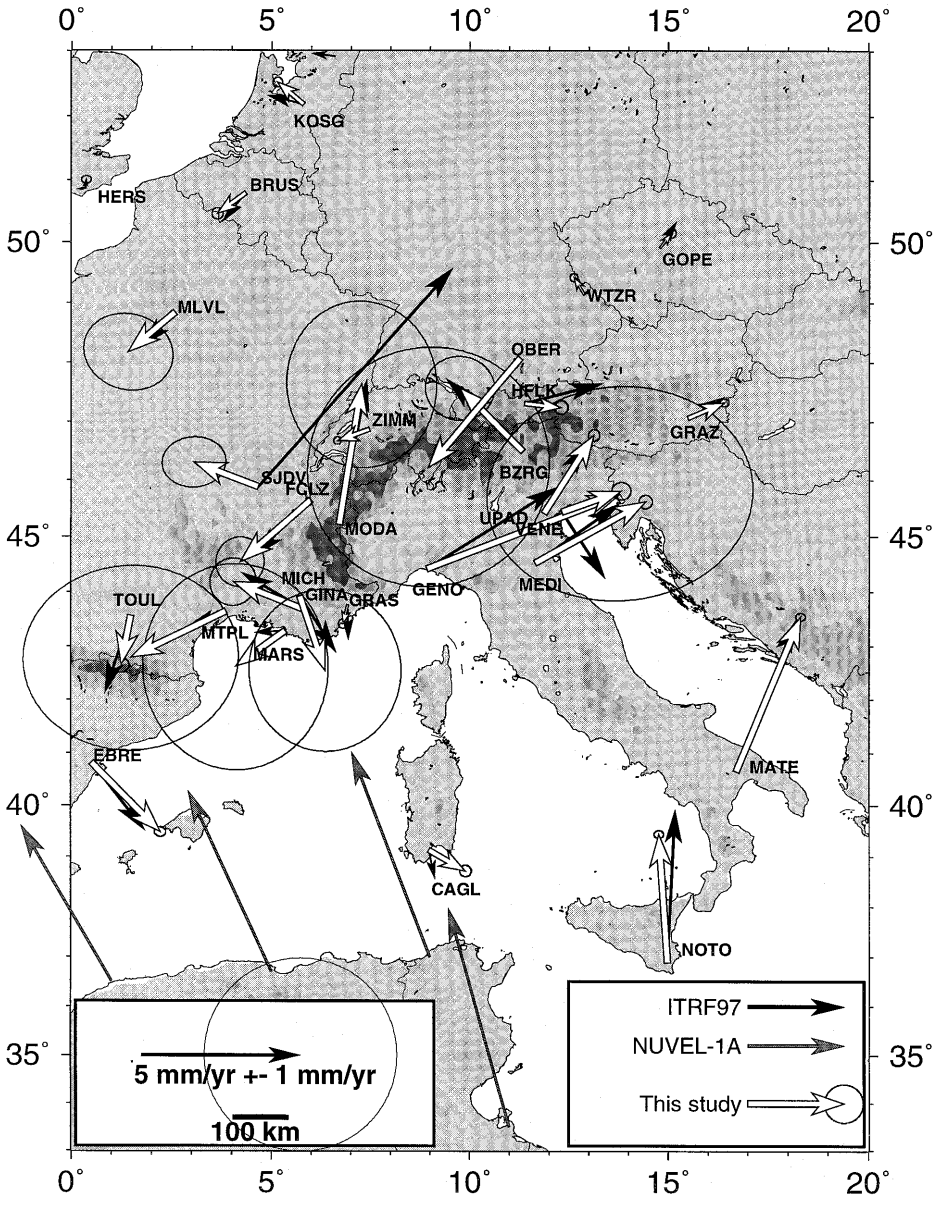

Fig. 4. Western European Network velocities. Velocities relative to the NNR-Nuvel-1A Eurasian plate for permanent GPS stations in Western Europe. *White arrows* depict present authors' solution. *Uncertainty ellipses* depict the 99% confidence level. *Black arrows* indicate the ITRF97 velocities (relative to NNR-Nuvel-1a Eurasian plate). *Thin gray arrows* on the African continent depict the African–Eurasian convergence predicted by the Nuvel-1A model

(Calais et al. 2000) shows a small rigid rotation between the two data sets. This rotation probably comes from the different techniques used to realize the reference frame. Once this rotation is subtracted, the two internal deformation patterns match very closely.

The agreement between permanent sites' and nearby ALPES sites' velocities is also good. Nevertheless, given the short time span of available data at the permanent sites, velocities determined from the full time series are more likely to be more accurate than epoch-like velocities. Indeed, at three sites where velocities agree reasonably well (FCLZ, MICH and SJDV), 'continuous' velocities match better nearby ALPES sites' velocities. Therefore, we use these continuous velocities to merge with the ALPES velocity field.

In all cases, the deviation from a rigid plate motion is small: the average residual velocity reaches 2 mm/yr with a maximum of 5 mm/yr at Matera. Such small numbers lie just at the limit of the confidence level of the data and therefore motions should be analyzed with care. Only the higher rates or site motions regionally coherent should be considered as reliable. Individual and local motions could be representative of true tectonic displacements but this cannot be assured with certainty with only two measurement epochs. In fact, a centering error of 5 mm (tribrach or antenna phase center offset, for example), on a given site, during either of the two campaigns, would map into a non-tectonic site velocity of 1 mm/yr. It is only after a third campaign is done that outlier position at a given epoch can be detected.

Despite their high uncertainties (relatively to their small velocities), a few important statements for Alpine tectonics can be inferred from the site velocities. First, there is no evidence for north–south shortening across the network, but rather for a widespread east–west extension. Using each site velocity and distance to the center of the network, we can construct the normal

Table 7. Velocities of European permanent stations (IGS, RGP, REGAL etc.) relative to NNR-Nuvel-1A Eurasia (mm/yr)

Site	ITRF97		ALPES solution		Difference
	Ve	*Vn*	*Ve*	*Vn*	
GRAZ	1.13	0.65	1.14	0.48	0.17
MATE	1.87	4.76	2.02	4.86	0.18
MODA	0.87	4.53	0.70	4.39	0.22
BRUS	−0.73	−0.91	−0.90	−0.66	0.30
UPAD	1.32	2.25	1.57	2.46	0.33
GINA	−1.95	1.17	−2.19	0.87	0.38
MLVL	−1.11	−1.12	−1.47	−1.25	0.38
GOPE	0.52	0.82	0.36	0.46	0.39
HERS	−0.27	−0.03	0.03	0.27	0.42
FCLZ	−1.82	−1.79	−2.22	−1.95	0.43
EBRE	1.68	−2.14	2.16	−2.19	0.48
BZRG	−2.42	2.25	−1.99	1.96	0.52
GRAS	0.02	−1.09	−0.14	−0.59	0.52
KOSG	−1.15	0.29	−0.83	0.70	0.52
WTZR	0.17	0.16	−0.32	0.54	0.62
MICH	1.15	−1.78	0.80	−2.35	0.67
MEDI	2.66	1.87	3.49	1.94	0.83
NOTO	0.24	4.83	−0.27	4.06	0.92
CAGL	0.19	−0.89	1.16	−0.67	0.99
TOUL	−0.81	−2.45	−0.30	−1.56	1.03
MARS	−0.95	−0.06	−1.56	−1.12	1.22
HFLK	2.46	0.63	1.15	−0.13	1.51
GENO	4.13	2.58	6.08	2.35	1.96
MTPL	−1.00	−0.35	−2.98	−1.46	2.27
VENE	1.35	−2.08	1.87	0.66	2.79
OBER	−0.39	−0.55	−2.91	−3.43	3.83
SJDV	6.12	6.86	−2.03	0.77	10.17

equations to estimate the constant bias term and the velocity gradient throughout the whole network, based on the formula of Feigl et al. (1990). Then the velocity gradient is used to form the average strain rate within the network. This method yields 3.5 nanostrain/yr oriented N116° and 0.02 nanostrain/yr on the perpendicular axis, located at the geometric center of the network. This corresponds to pure extension perpendicular to the mountain range axis (Fig. 5). Second, there is no clear distinct motion of the Corso-Sardinian block towards north (the Corso-Sardinian indentor motion). If this block is moving, its motion is a rotation, the first effect of which is accentuated opening in the Tyrrhenian Sea, which is classically associated with slab rollback in the Apennines (Kastens et al. 1988).

Within the Alpine range, the area of maximum extension lay in the southern part of the network (4 mm/yr between points PRN0 and CLB0-CHA0), on the Piemont arc, at the exact location of a very seismically active strip (Sue et al. 1999). Another zone of milder extension can be dectected further north and slightly west (2–3 mm/yr between points CFE0, MTC0 and AUS) near the Briançonnais arc, also seismically active (Sue et al. 1999). This extension is coherent with the work of Sue et al. (2000) who have locally found extension in the Briançonnais seismic arc area by comparing old triangulation to more recent GPS measurements.

Coherent block behavior can also be detected. Six points (PEC0, CHA0, VER0, SJU0, CBR0 and ROV0) show a coherent motion towards the west at 1–2 mm/yr. This block could be identified with the Provence block. BAU0 and MPA0 within the Maures massif show a coherent compressive motion towards the north and the rest of Provence.

Finally, the Italian points SGG0, NIV0, LAU0 and PRN0 show a coherent anticlockwise rotation, which could be representative of the one of the occidental Po plain. The velocity of the permanent site at Genova is compatible with this rotation, although it is somewhat larger, but with a far larger uncertainty due to its shorter time series.

The remaining points, mostly in the northern part of the network, hardly show any significant motion. However, they collectively contribute to the overall east–west extension tendancy.

5 Tectonic interpretation

Keeping in mind that differential motions in the Western Alps obtained by GPS are low and therefore subject to improvements, we attempt here to interpret our results in the framework of the Africa–Eurasia collision. The first problem to address is the lack of N–S shortening of the Western Alps (<1 mm/yr on 500 km). This could be interpreted as the result of a modest convergence between Africa and Europe. The African motion with respect to Europe defined by the NNR–NUVEL1A model is 9 mm/yr oriented 10°W in the Eastern Mediteranean and 6 mm/yr oriented 25°W in the Western Mediteranean. A few GPS sites were measured on the north of the African plate between 1994 and 1998. The motion of sites in Egypt is 5.5 mm/yr oriented

20°W (McClusky et al. 2000). On the western part of the plate, we find a motion of Mas Palomas (Canaries Islands) of 3 mm/yr oriented 30°W. Therefore, the relative instantaneous motion of the African plate with respect to Eurasia at 6°W longitude is expected to be around 4 mm/yr oriented 25°W. Because the north component of most of the GPS points within the western alpine belt and in the Corsica–Sardinia block is nearly 0 mm/yr with respect to Eurasia, the interpretation that arises is that most of the Africa–Eurasia shortening is accomodated in moutains belts of northermost Africa. A 25°W shortening direction in the Maghrebids is consistent with the NW-trending slip vectors from thrust earthquakes between Gibraltar and Sicily (Argus et al. 1989), such as the 10 October 1980, El Asnam earthquake (Yielding et al. 1985). Such an interpretation implies that the closure of the Ligurian sea between Corsica and the southern alpine margin could be mild despite the occurrence of recent earthquakes (Bethoux et al. 1992). Even more surprising is the western displacement at 1–2 mm/yr of most of the sites belonging to the western part of the GPS Alps network (Morvan, Massif Central, Provence) with respect to central Europe and the Adriatic plate. Together with the lack of N–S compression, this would imply that the Western Alps are submitted to a widespread extension. Until now, earthquake focal mechanisms have revealed that E–W extension in the internal Alps is a narrow (10–40-km) band corresponding to the highest topography (Mercantour, Briançonnais arc). At the latitude of Torino, earthquake focal mechanisms also reveal that the Po plain in the east as well as the external massifs in the west are likely to be in E–W compression (Eva et al. 1997; Sue et al. 1999). Our geodetic analysis therefore indicates that normal faulting in the core of the Alps dominates thrust faulting at the present day. However, this extension is mild compared to the one occuring in the central Apennines where GPS surveys have revealed 5 mm/yr of extension normal to the belt (D'Agostino et al. 2001). Various mechanisms could be responsible for the extension of the Western Alps [see Sue et al. (1999) for a complete discussion]. A first solution is to invoke a gravitational origin, and a mountain collapse. However, the modest elevation of the Alps (1500 m) may not be compatible with the onset of this mechanism. Another solution is to invoke the weight of the European lithosphere, which could act like a slab pull force and would induce tensional forces in the upper crust above.

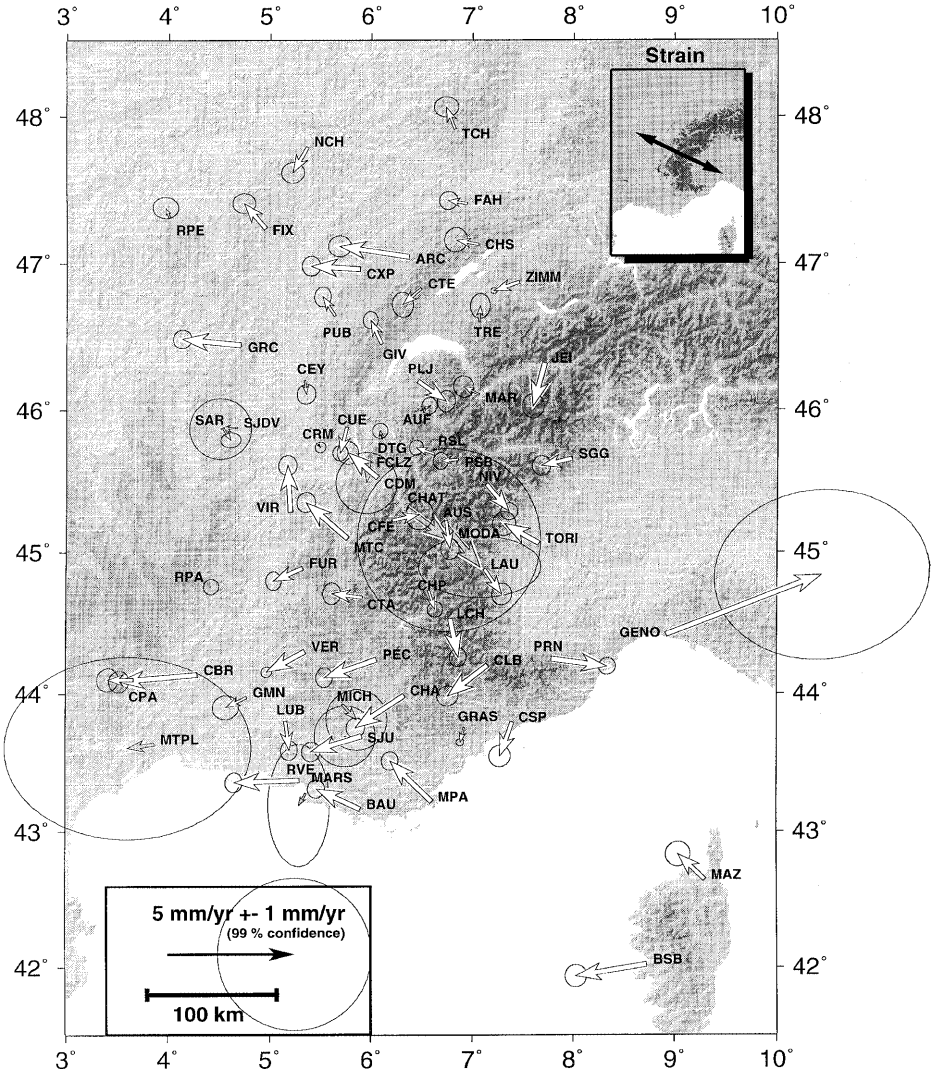

Fig. 5. GPS ALPES velocities. *White arrows* depict for the ALPES 1993–1998 sites. *Gray arrows* depict the velocities at permanent sites (REGAL, RGP and IGS) obtained from their continuous time series. *Uncertainty ellipses* depict the 99% confidence level. The inset in the upper-right corner depicts the principle axis of the strain vector (mainly extensional)

A final hypothesis is to consider that the Western Alps are extending in response to horizontal forces around. If we consider that Africa is moving towards Europe at 25°W, this results in a force pulling Europe to the northwest direction. Because Europe is crossed by a N–S band displaying present day E–W extension (Rhine graben, Bresse Graben, Limagne, Briançonnais arc, Mercantour), it is reasonnable to propose that the African motion may result in the slow dislocation of Western Europe thanks to a N–S weakness zone. The assessment of this hypothesis will require a careful analysis of the increasing GPS data set in westernmost Europe.

6 Conclusion

When processed with great care and precision, two GPS campaigns over a 5-year time span allow us to determine small but non-negligible motions in the Western Alps. Despite the overall shortening of 6 mm/yr between Africa and Eurasia (Fig. 4), the Western Alps seems to deform with radial (E–W) extension, especially in its southern part. North–South compression is not detectable at a level >1 mm/yr, excepted in the southermost alpine margin near the Maures Massif. These differential motions are compatible with recent seismological analysis in the Southern Alps (Sue et al. 1999; Baroux et al. in press), and the more recent permanent GPS network in the area (Calais 1999; Calais et al. 2000). Nevertheless, it should be remembered that 2 mm/yr motion relies on a 1-cm displacement detected over a 5-year period. Such a displacement is quite small and individual site motions could reveal errors of at least 50%. A consequence of this is that local short-scale motions detected by site-to-site relative motions are not reliable and should not be used to put lower or upper bounds on specific faults. In particular, these data should not be use directly to assess seismic hazards on faults in the south-east part of France ('moyenne Durance' fault, 'Nimes' fault, 'Cévennes' fault). It is only when a third campaign, due in 2003, is done that individual site motion will be confirmed or revised.

Acknowledgments. We are grateful to everyone involved in the long-term collaboration on the GPS–ALPES project since 1991. Special thanks to all surveyors from many different French, Italian, and Swiss institutes. Special thanks to C. Sue, whose detailed review greatly helped in improving the paper. The bulk of this work has been achieved to a large part in the framework of the Tectoscope-Positionnement program in 1993 and the GeoFrance-3D program in 1998, and sponsored by the INSU–CNRS, BRGM, CEA/LDG, CERGA, CNES, EDF, ESGT, ETH (Zurich), IGN, ING (Roma) and IPSN.

References

Argus D, Gordon R, Demets C, Stein S (1989) Closure of the Africa Eurasia North America plate motion circuit and tectonics of the Gloria fault. J Geophys Res 94: 5585–5602

Baroux E, Béthoux N, Bellier O (2001) Analyses of the stress field in southeastern France from earthquake focal mechanisms. Geophys J Int 145: 336–348

Béthoux N, Frechet J, Guyoton F, Thouvenot F, Cattaneo M, Eva C, Nicolas M, Granet M (1992) A closing Ligurian sea. Pure Appl Geophys 139: 179–194

Beutler G, Kouba J, Springer T (1993) Combining the orbits of the IGS processing centers. In: Kuba J (ed) Ottawa, Canada. Proc IGS analysis center workshop, pp 20–56

Boucher C, Altamimi Z, Sillard P (1999) The 1997 International Terrestrial Reference Frame (ITRF97). IERS tech note 27, Observatoire de Paris

Calais E (1999) Continuous GPS measurements across the western Alps, 1996–1998. Geophys J Int 38: 221–230

Calais E, Bayer R, Chéry J, Cotton F, Doerflinger E, Flouzat M, Jouanne F, Kasser M, Laplanche M, Maillard D, Martinod J, Matthieu F, Nicolon P, Nocquet J-M, Scotti O, Serrurier L, Tardy M, Vigny C (2000) REGAL: a permanent GPS network in the western Alps and foreland, first results. C R Acad Sci No 7, October pp 435–442

D'Agostino N, Giuliani R, Mattone M, Bonci L (2001) Active crustal extension in the central Apennines (Italy) inferred from GPS measurements in the interval 1994–1999. Geophys Res Lett 28: 2121–2124

DeMets C, Gordon RG, Argus D, Stein S (1994) Effect of recent revisions to the geomagnetic reversal time scale on estimates of current plate motions. Geophys Res Letters 21: 2191–2194

Eva E, Solarino S, Eva C, Neri G (1997) Stress tensor orientation derived from fault plane solutions in the southwestern Alps. J Geophys Res 102: 8171–8185

Feigl KL, King RW, Jordan TH (1990) Geodetic measurement of tectonic deformation in the Santa Maria fold and thrust belt, California. J Geophys Res 104: 2679–2699

Ferhat G, Feigl KL, Ritz JF, Souriau A (1998) Geodetic measurement of tectonic deformation in the southern Alps and Provence, France, 1947–1994. Earth Planet Sci Lett 159: 35–46

Herring TA (1999) Documentation for the GLOBK software version 5.01. Massachussetts Institute of Technology, Cambridge, MA

Kastens K, Mascle J, Auroux C, Bonatti E, Broglia C, Channell J, Curzi P, Emeis K, Glacon G, Hasegawa S, Hieke W, Mascle G, McCoy F, McKenzie J, Mendelson J, Mueller C, Rehault J-P, Robertson A, Sartori R, Sprovieri R, Torii M (1988) ODP LEG-107 in the Tyrrhenian sea – insights into passive margin and back-arc basin evolution. Geol Soc Am Bull 100: 1140–1156

King RW, Bock Y (1999) Documentation for the GAMIT GPS software analysis version 9.9. Massachussetts Institute of Technology, Cambridge, MA

McClusky S, Balassanian S, Barka A, Demir C, Ergintav S, Georgiev I, Gurkan O, Hamburger M, Hurst K, Kahle H, Kastens K, Kekelidze G, King R, Kotzev V, Lenk O, Mahmoud S, Mishin A, Nadariya M, Ouzounis A, Paradissis D, Peter Y, Prilepin M, Reilinger R, Sanli I, Seeger H, Tealeb A, Toksoz M, Veis G (2000) Global Positioning System constraints on plate kinematics and dynamics in the eastern Mediterranean and Caucasus. J Geophys Res 105: 5695–5719

Neilan R (1995) The evolution of the IGS global network, current status, and future aspects. In: Zumberge JF et al. (eds) Pasadena JPL, CA, USA IGS annual report, JPL publ 95-18, pp 25–34

Rothacher M, Mader G (1996) Combination of antenna phase center offsets and variations: antenna calibration set $IGS_0$1. IGS Central Bureau/University of Berne

Rothacher M, Mervart L (1996) BERNESE GPS software version 4.0. Astronomical Institute, University of Berne

Schmidt SM, Kissling E (2000) The arc of the western Alps in the light of geophysical data on deep crustal structure. Tectonics 19: 62–85

Sue C, Tricart P (1999) Late Alpine brittle extension above the frontal pennine thrust near Briançon, western Alps. Eclogae Geol Helv 92: 171–181

Sue C, Thouvenot F, Fréchet J (1999) Widespread extension in the core of the western Alps revealed by earthquake analysis. J Geophys Res 104: 25 611–25 622

Sue C, Martinod J, Tricard P, Thouvenot F, Gamond J-F, Fréchet J, Marinier D, Glot J-P, Grasso J-R (2000) Active deformation in the inner western Alps inferred from comparison between 1972-classical and 1996-GPS geodetic surveys. Tectonophysics 320: 17–29

Thomas JC, Claudel ME, Collombet M, Tricart P, Chauvin A, Dumont T (1999) First paleomagnetic data from the sedimentary cover of the French Penninic Alps: evidence for Tertiary counterclockwise rotations in the Western Alps. Earth Planet Sci Lett 171: 561–574

Yielding G (1985) Control of rupture by fault geometry during the 1980 El-Asnam (Algeria) earthquake. Geophys J R Astron Soc 81: 641–670